Acoustic Emission-Based Identification of Discontinuous Plastic Flow in Austenitic Stainless Steels

J. TABIN, H. NEJMAN, A. SZYSZKO, Z. RANACHOWSKI, and J. KAWAŁKO

Discontinuous plastic flow (DPF) in austenitic stainless steels at cryogenic temperatures is typically identified by serrated stress–strain responses. Here, acoustic emission (AE) is used to probe deformation during uniaxial tensile tests of 304, 316L, and N50 steels at 4 K. Pronounced AE activity is detected well before stress drops, revealing discrete precursor events. The results show that DPF is preceded by progressive microstructural reorganization and establish AE as a sensitive tool for identifying plastic instability.

https://doi.org/10.1007/s11661-026-08252-6

AUSTENITIC stainless steels (ASS), including the AISI 304, AISI 316L, and N50 grades, combine high mechanical performance with excellent corrosion resistance across a broad temperature range. These properties make them key structural materials in demanding applications such as automotive and aerospace engineering, nuclear and chemical processing, as well as space and superconducting technologies, where components are exposed to conditions ranging from ambient temperature down to cryogenic and near-zero-kelvin regimes.[1,2]

Discontinuous plastic flow (DPF) is a characteristic deformation instability observed in many metallic alloys, including AISI 304, AISI 316L at cryogenic temperatures, below T_0 or T_1.[3] It manifests as serrated stress–strain curves and localized plastic deformation, which can strongly affect mechanical stability in cryogenic applications. Despite extensive research, the physical origin of DPF has long remained controversial, and several complementary mechanisms have been proposed.

Early interpretations emphasized thermal effects, suggesting that limited heat conduction at very low temperatures leads to local temperature rises and sudden stress drops.[4] Other studies proposed analogies to dynamic strain aging (DSA), where repeated pinning and release of dislocations by solute atoms produce oscillatory flow.[5] However, classical diffusion-controlled mechanisms are strongly suppressed at cryogenic temperatures, limiting the applicability of conventional DSA concepts. Additional explanations linked DPF to deformation twinning and strain-induced phase transformations, arguing that abrupt microstructural changes destabilize plastic flow.[6] While these mechanisms are frequently observed during cryogenic deformation, they do not fully explain the spatial and temporal characteristics of DPF.

Increasing experimental evidence supports a dislocation-controlled origin of DPF. At cryogenic temperatures, reduced stacking fault energy and limited cross-slip promote the accumulation of dense dislocation pile-ups, particularly of edge dislocations, at grain and subgrain boundaries. As deformation proceeds, these pile-ups grow until a critical stress state is reached, leading to their sudden collective release.[3,7] This process produces a characteristic serration on the stress–strain curve that can be divided into successive stages: quasi-elastic loading, plastic flow associated with dislocation accumulation, an abrupt stress drop caused by a dislocation avalanche and strain localization, and, in some cases, a subsequent stress-relaxation stage before the next loading cycle.[8,9]

The collective release of dislocations from pre-existing dislocation blocks gives rise to localized plastic deformation manifested as macroscopic shear bands.[10] Full-field strain measurements reveal that these bands propagate along structured, often bidirectional paths, reflecting strong spatiotemporal correlations between successive dislocation-block activation events.

The handling Editor for this article was Matthias Militzer and the handling Associate Editor was Kester D. Clarke.

J. TABIN, H. NEJMAN, A. SZYSZKO, and Z. RANACHOWSKI are with the Institute of Fundamental Technological Research, Polish Academy of Sciences, 02-106 Warsaw, Poland. Contact e-mail: jtabin@ippt.pan.pl J. KAWAŁKO is with the Academic Centre for Materials and Nanotechnology, AGH University of Krakow, 30-059 Krakow, Poland.

Manuscript submitted February 11, 2026; accepted April 29, 2026.

Published online: 19 May 2026

Dislocation blocks act as metastable reservoirs of stored elastic energy: their progressive growth and interconnection increase local stress heterogeneity until a critical threshold is exceeded, triggering an avalanche-like release of dislocations. Local temperature rises are detected only after shear-band formation, demonstrating that heating is a consequence rather than a trigger of DPF; the associated thermal softening locally stabilizes the microstructure and suppresses further propagation. Microstructural observations show that the collapse and reorganization of dislocation blocks within shear bands are accompanied by strain-induced martensitic transformation, deformation twinning, and transient grain refinement. Overall, DPF is best described as a collective dislocation-avalanche process controlled by the nucleation, growth, and collapse of dislocation blocks under microstructural constraints and cryogenic thermal conditions. Recent high-resolution studies indicate that the macroscopic stress drop associated with discontinuous plastic flow is preceded by a hierarchy of micro- and meso-scale deformation processes. In particular, Kim *et al.*[11] demonstrated by means of digital image correlation (DIC), that small stress fluctuations and localized strain-rate heterogeneities systematically appear prior to the main serration, reflecting the progressive build-up of hierarchical dislocation networks at cryogenic temperatures. These observations suggest that serrations represent the final stage of an extended preparatory process rather than an instantaneous instability.

Until now, the identification of DPF has been based on force measurements, extensometers, temperature sensors and full-field techniques such as DIC; however, the potential of acoustic emission for resolving and identifying successive stages of DPF evolution has not yet been systematically explored.

Acoustic emission (AE) is a passive, non-destructive technique widely used to monitor plastic deformation in metallic materials.[12–14] AE originates from the sudden release of elastic strain energy during irreversible microstructural events and is recorded as transient elastic waves. Because plastic deformation in ASS at cryogenic temperatures develops through localized and discontinuous mechanisms, AE is particularly effective for real-time detection of plastic activity. Numerous studies have shown that AE activity accompanies plastic flow across different alloys and crystal structures, confirming its strong link to fundamental deformation mechanisms such as PLC,[12] Lüders band propagation,[15] or deformation-induced phase transformation.[16,17] Furthermore, AE is widely applied to monitor microstructural evolution during heat treatment process, such as recovery, recrystallization, and phase transformation.[18,19] In these cases, AE reflects dislocation-mediated strain accommodation rather than slow diffusion processes. Nevertheless, it is lack of example when AE was used to identify mechanical behavior of metastable materials at temperature near 0 K.

This work demonstrates, for the first time, that acoustic emission activity develops well in advance of the stress drops associated with DPF. These precursor signals precede the macroscopic manifestation of instability and are not captured by the conventional stress–strain response. The results indicate that measurable AE activity occurs prior to the onset of large-scale shear banding, pointing to the presence of precursor processes. This finding motivates a reassessment of existing DPF models and highlights the need to incorporate such precursor activity in the description of serrated flow.

Commercial sheets of 304 and 316L austenitic stainless steels, with a thickness of 2 mm, are used in the present study. The chemical composition of the 304 steel is (in wt pct) C 0.07 pct, Cr 18 pct, Ni 10 pct, Mn 2 pct, and Si 0.8 pct. The 316L steel has a composition of C 0.03 pct, Cr 18.2 pct, Ni 11.5 pct, Mn 2 pct, Mo 2 pct, and Si 1.0 pct. Dog-bone-shaped tensile specimens are fabricated using electrical discharge machining (EDM) from the commercial sheets, with the tensile axis aligned with the rolling direction. The semi-products are supplied in the annealed and lightly cold-rolled conditions (304 and 316L) in accordance with ASTM A480 and EN 10088 standards and represent materials commonly used for structural components operating over a wide temperature range.[2] In addition, an N50 austenitic stainless steel is investigated. The N50 specimens are cut by EDM from a bulk block that was hot-forged, solution-annealed, and water-quenched prior to machining. The chemical composition of the N50 steel (in wt pct) is C 0.02 pct, Si 0.32 pct, Mn 5.68 pct, Cr 20.96 pct, Ni 13.28 pct, P 0.022 pct, S 0.001 pct, Mo 2.34 pct, V 0.23 pct, Al 0.033 pct, Co 0.04 pct, Nb 0.18 pct, B 0.0041 pct, and N 0.32 pct. N50 is included as a reference material, as it remains a stable austenitic steel at 4 K and does not exhibit discontinuous plastic flow (DPF).

The initial microstructure of the as-received materials in all cases consists of equiaxed, fully recrystallized grains with recrystallization twins present in some of the larger grains (Figure 1). The average grain size is comparable in the 304 and 316L steels, measuring 16.0 μm and 14.3 μm, respectively, whereas the N50 steel exhibits a significantly coarser microstructure with an average grain size of approximately 55.0 μm (Figure 1).

Displacement-controlled uniaxial tensile tests were performed on dog-bone specimens of 304, 316L, and N50 austenitic stainless steels at 4 K with a crosshead velocity of 1 mm/min. The specimen was tensile tested up to a predefined deformation level [Figures 2(a), (c), and (e)], while force, elongation, and AE signals were continuously recorded. The test was then interrupted, and the specimen was removed from the cryostat. Subsequently, the volume fraction of deformation-induced martensite (DIMT) along the gauge length was measured using a ferritscope - Fisher FMP30 [Figures 3(b) and (f)]. Based on this distribution, regions located before and after the martensitic transformation front were identified in 316L specimen. These regions were then analyzed by EBSD, revealing ex situ differences in both martensite content and active deformation mechanisms associated with DPF [Figures 3(d) and (e)].

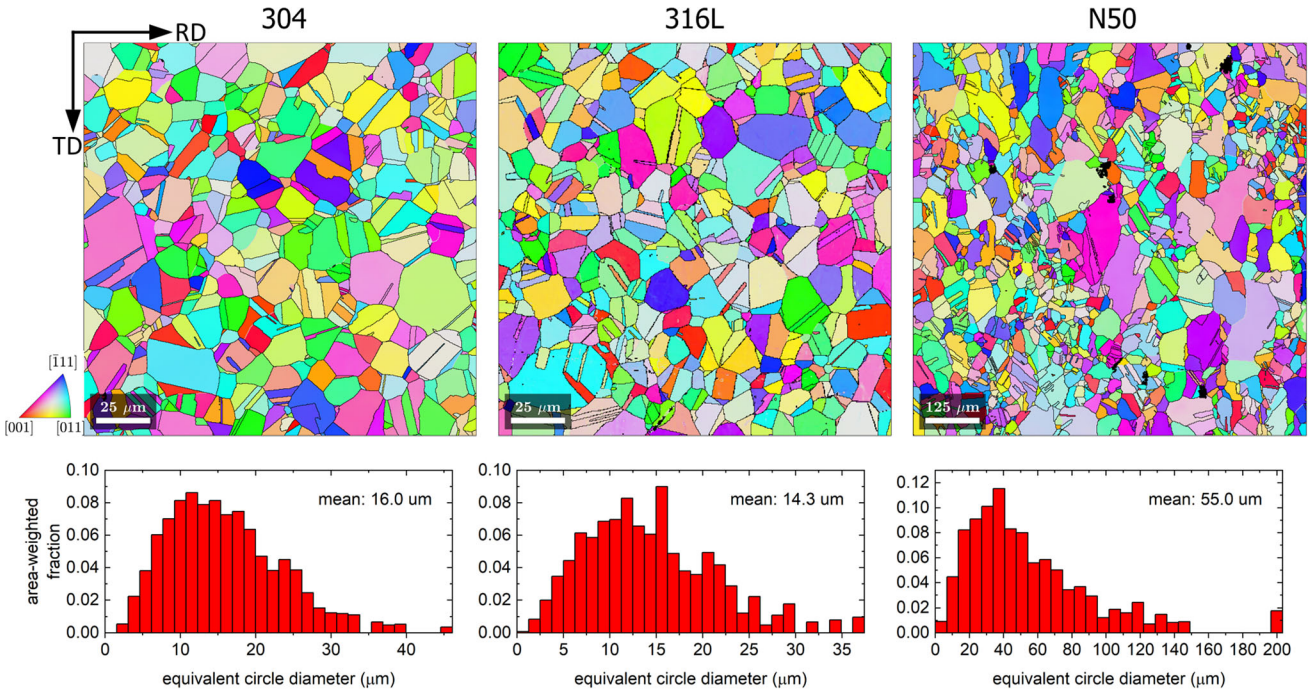

Fig. 1—The microstructures of the investigated materials, as received, are shown in the top row as inverse pole figure (IPF) maps. IPF coloring relative to the ND axis. The bottom row displays the grain size distributions in terms of equivalent circle diameter (Color figure online).

Acoustic emission (AE) signals were recorded using a low-temperature AE sensor (AE154D, Physical Acoustics Corporation) mounted on the cryostat rod, which served as a waveguide transmitting elastic waves from the specimen to the sensor (Figure 4).

The AE signal chain included a low-noise preamplifier (62 dB), a high-pass filter (5 kHz), and an A/D converter with a sampling frequency of 250 kHz. Time–frequency characteristics of AE activity were analyzed using continuous windowed FFT and presented in the form of color spectrograms (Figure 2).

The AE spectrograms (Figure 2) show distinct burst-type activity occurring well before the abrupt stress drop associated with a serration. These bursts are visible both in the full-test spectrograms [Figures 2(a), (c), and (e)] and in the magnified views of individual serrations [Figures 2(b), (d), (f)]. Importantly, they appear during plastic deformation in the macroscopic stress–strain response, indicating the presence of localized deformation processes that precede the macroscopic instability. The observed pre-serration AE activity is itself intermittent and discontinuous, demonstrating that the preparatory stage of DPF does not correspond to smooth, continuous plastic flow. Instead, it consists of a sequence of localized instability events that progressively prepare the system for the subsequent macroscopic serration.

In addition to the metastable austenitic steels 304 and 316L, the present work also includes results obtained for N50 steel tested at 4 K. In contrast to 304 and 316L, N50 does not exhibit stress serrations under these conditions. The absence of discontinuous plastic flow in N50 provides a valuable reference case, enabling a direct comparison of AE spectrograms recorded during serrated and non-serrated deformation. This comparison demonstrates that burst-type AE activity is also present in N50 steel; however, in contrast to 304 and 316L, these bursts are distributed over the entire duration of deformation and across the full extent of the AE spectrogram. In the metastable steels, the burst-type activity becomes strongly concentrated immediately prior to the abrupt stress drop, whereas in N50, no such temporal clustering is observed. Consequently, the AE response reflects differences in the underlying strain localisation mechanisms and their temporal organization, rather than merely the occurrence of plastic flow itself. Such pre-serration AE activity in 316L and 304 can be associated with the development of micro-scale shear localization. At room temperature, strain localization in FCC polycrystals is known to be preceded by the formation of micro- and meso-shear bands. Nalepka *et al.*[20] showed that, in metastable 304 steel, a macroscopic strain front forms only after extensive microstructural reorganization. During this process, austenite grains rotate toward Cu and Goss–Brass (GB) components, which favor intense shear and promote deformation-induced martensitic transformation. As a result, a gradient between compliant and stiff regions is created, enabling stable front propagation. The strain front itself consists of meso-shear bands formed by joined shear systems within Cu/GB grain chains.[20] Classical studies further demonstrate that macroscopic shear bands in FCC metals develop through crystallography-controlled lattice rotations aligning {111} slip planes with the shear plane, while microstructural deflection or kink bands act as their precursors.[21]

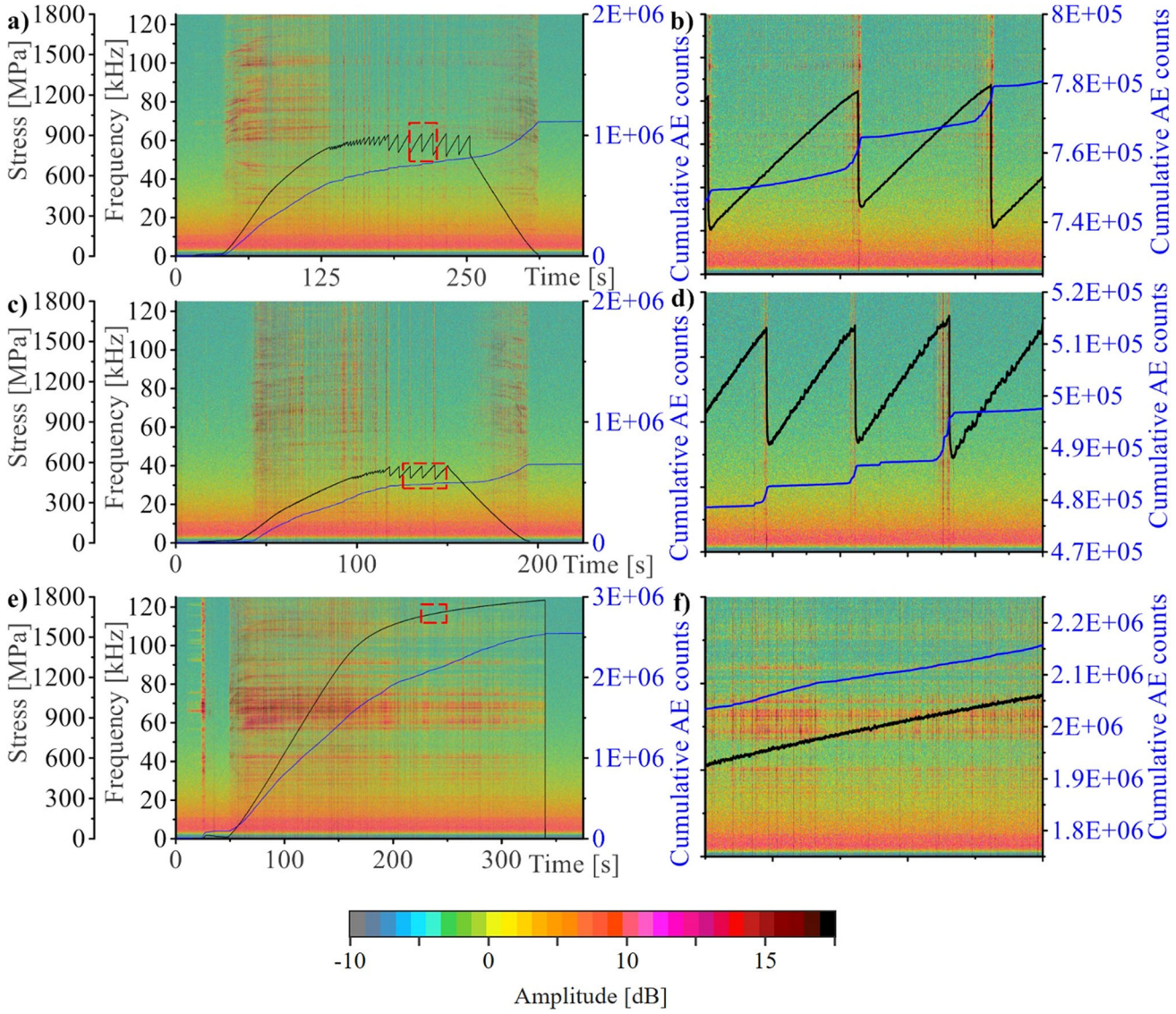

Fig. 2—Uniaxial tensile tests of 316L, 304, and N50 at 4 K. Time-resolved stress response (black) and cumulative AE counts (blue) with corresponding AE spectrograms for 316L (*a*), 304 (*c*), and N50 (*e*); enlarged AE spectrograms of representative single serrations for 316L (*b*), 304 (*d*), and N50 (*f*) (Color figure online).

Micro- and meso-scale shear localization has also been reported at cryogenic temperatures. Nalepka *et al.*[22] demonstrated that deformation at extremely low temperatures involves a multiscale mechanism, including micro-shear bands, twin-boundary formation, and classical lattice barriers such as Lomer–Cottrell locks. In this framework, micro-shear bands may form when local barriers are overcome under critical resolved shear stress. These observations are compatible with the thermo-mechanical description of discontinuous plastic flow (DPF) proposed in Reference 10 which focuses on the formation and propagation of localized deformation zones during serrations. However, the framework in Reference 10 primarily addresses the stages associated with the abrupt stress drop and subsequent evolution, while deformation activity occurring prior to the first stress drop is not explicitly considered. Finally, presented results are consistent with the thermally induced dislocation-dynamics model of DPF,[11] where discontinuous deformation at cryogenic temperatures is governed by the progressive activation of hierarchical dislocation networks and precursor avalanches.

In this context, the early AE bursts observed in the present study can be interpreted as signatures of discrete microstructural events preceding the macroscopic serration. Their timing and characteristics are consistent with the nucleation and early organization of micro- and meso-shear bands, rather than with the collapse of dislocation blocks associated with later stages of DPF. This suggests that micro-scale shear localisation represents an additional, earlier stage in the development of DPF. The present results therefore complement existing DPF models by showing that AE provides access to pre-serration deformation processes that are not captured by the macroscopic stress–strain response.

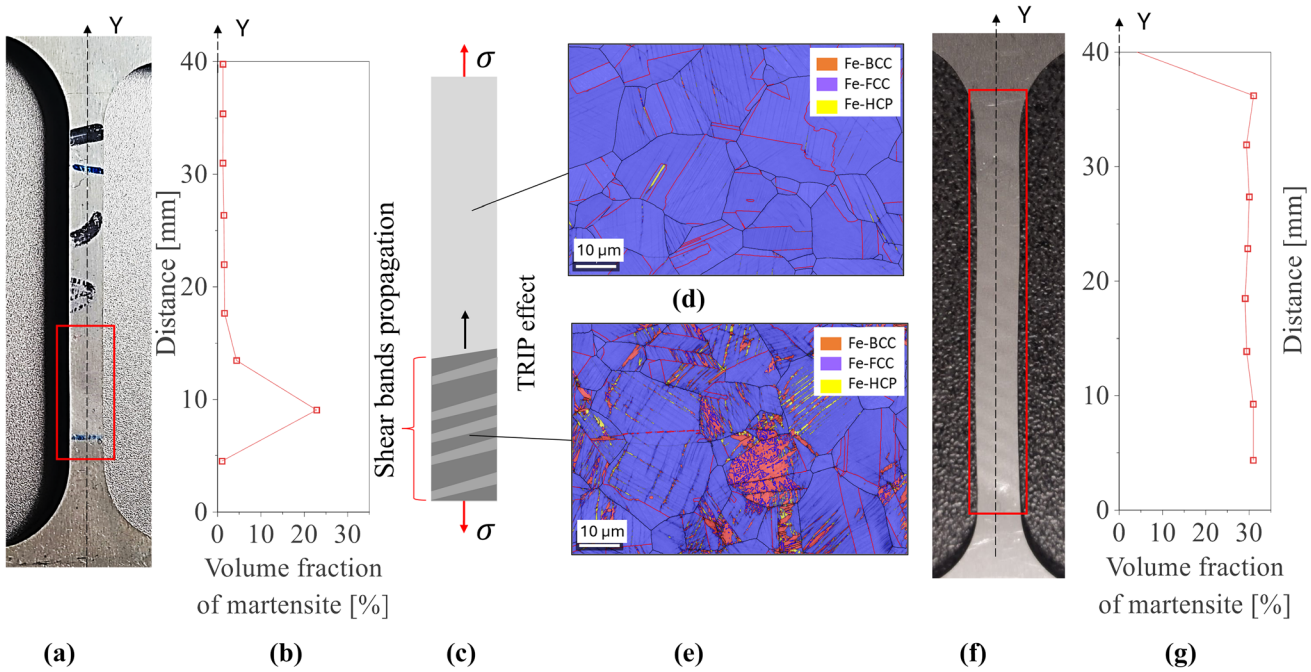

Fig. 3—Propagation of macroscopic shear bands during discontinuous plastic flow (DPF) in 316L under displacement-controlled uniaxial tension at 4 K: (*a*) initiation of a shear band at the lower part of the specimen; (*b*) distribution of deformation-induced martensite (DIMT); (*c*) schematic illustration of shear-band propagation during DPF; (*d*) phase distribution map for the region ahead of the shear band; (*e*) phase distribution map for the region behind the shear band; (*f*) specimen showing the propagation path of the shear band during DPF; (*g*) distribution of deformation-induced martensite (DIMT).

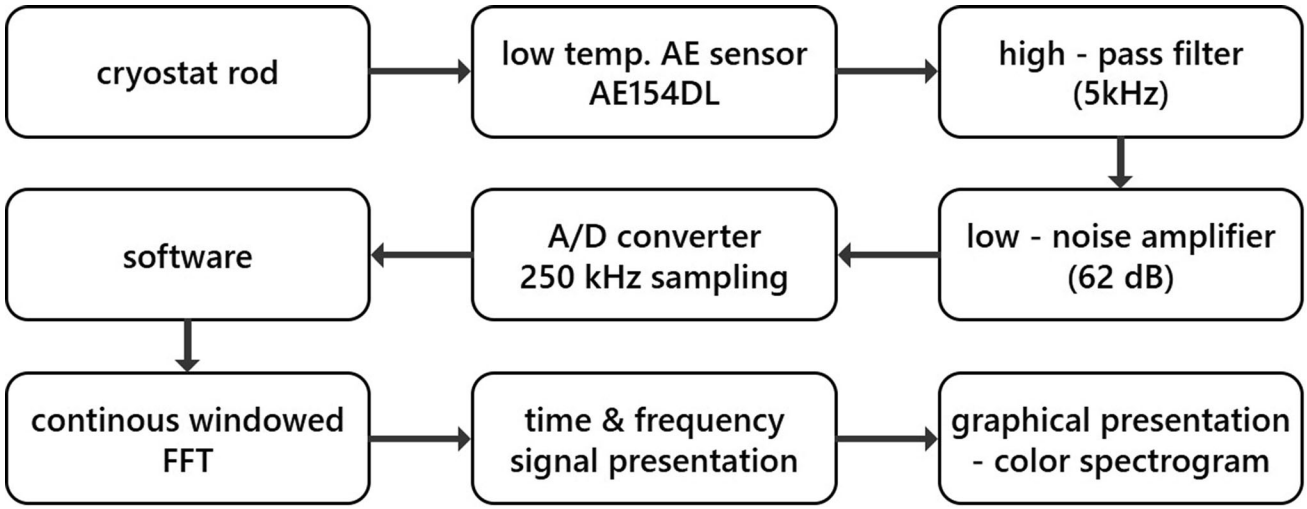

Fig. 4—Schematic of the acoustic emission (AE) measurement system used during uniaxial tensile testing at 4 K, including the cryostat rod acting as a waveguide, AE sensor, signal conditioning, data acquisition, and time–frequency analysis.

Currently, work is underway on a detailed SEM–EBSD analysis aimed to identify the underlying plastic deformation mechanisms in the tested materials. The EBSD results will enable direct correlation between the observed AE spectrograms and microstructural features such as slip system activation, deformation twinning, shear-band formation, and strain-induced phase transformation. In this way, the AE signatures will be quantitatively linked to the mechanisms of plastic deformation operating at cryogenic temperatures in metastable austenitic steels 304 and 316L, as well as in the non-serrating N50 steel, providing a unified microstructure-based interpretation of the spectrograms.

This work has been supported by the National Science Centre through the Grant No 2023/51/D/ST8/02370. The authors would like to express their gratitude to the A. Brodecki and M. Wyszkowski for technical support.

On behalf of all authors, the corresponding author states that there is no conflict of interest.

OPEN ACCESS

REFERENCES

1. F. Bertinelli, F. Fudanoki, T. Komori, G. Peiro, and L. Rossi: *IEEE Trans. Appl. Supercond.*, 2006, vol. 16, pp. 1773–76.
2. P. Fernández-Pisón, J.A. Rodríguez-Martínez, E. García-Tabarés, I. Avilés-Santillana, and S. Sgobba: *Eng. Fract. Mech.*, 2021, vol. 258, p. 108042.
3. B. Obst and A. Nyilas: *Mater. Sci. Eng., A*, 1991, vol. 137, pp. 141–50.
4. Z.S. Basinski: *Proc. R. Soc. Lond. Ser. A*, 1957, vol. 240, pp. 229–42.
5. P. Hähner and M. Zaiser: *Acta Mater.*, 1997, vol. 45, pp. 1067–75.
6. J. Liu, X. Guo, Q. Lin, Z. He, X. An, L. Li, P.K. Liaw, X. Liao, Y. Liping, L. Junpin Lin, J.R. Xie, and Y. Zhang: *Sci. China Mater.*, 2019, vol. 62, pp. 853–63.
7. A. Seeger in *An International Conference Held at Lake Placid*, ed. by J.C Fisher, (Wiley, New York, 1957).
8. B. Skoczeń: *J. Theor. Appl. Mech.*, 2008, vol. 46, pp. 949–71.
9. J. Tabin: *Mech. Mater.*, 2021, vol. 163, p. 104090.
10. L. Xie, H. Zhang, J. Xin, F. Shen, Z. Geng, M. Jiang, Z. Huang, B. Li, W. Wang, C. Huang, and L. Li: *Commun. Mater.*, 2025, vol. 6, p. 159.
11. Y.S. Kim, T. Kang, S.K. Hong, J. Brechtl, M. Lebyodkin, Y.H. Cheng, E.W. Huang, P.K. Liaw, S. Harjo, W. Gong, and C.Y. Chiang: *Acta Mater.*, 2025, vol. 292, p. 120970.
12. F. Chmelík, F.B. Klose, H. Dierke, J. Šachl, H. Neuhäuser, and P. Lukáč: *Mater. Sci. Eng., A*, 2007, vol. 462, pp. 53–60.
13. A. Vinogradov and P. Döring: *J. Alloy. Compd.*, 2025, vol. 1044, p. 184518.
14. Y. Chen, B. Gou, X. Xu, X. Ding, J. Sun, and E.K. Salje: *Add. Manuf.*, 2023, vol. 78, p. 103819.
15. A.A. Asmaa, D. Lajos, Z.T. László, V.K. Irina, I.C. Yuriy, and L.B. Dezső: *J. Alloy. Compd.*, 2025, vol. 1027, p. 180507.
16. A. Vinogradov, A. Lazarev, M. Linderov, A. Weidner, and H. Biermann: *Acta Mater.*, 2013, vol. 61, pp. 2434–49.
17. P. Haušild, V. Davydov, J. Drahokoupil, M. Landa, and P. Pilvin: *Mater. Des.*, 2010, vol. 31, pp. 1821–27.
18. E.A. Pieczyska, H. Tobushi, K. Takeda, D. Stróz, Z. Ranachowski, K. Kulasinski, S. Kúdela Jr., and J. Luckner: *Kovove Mater.*, 2012, vol. 50, pp. 309–18.
19. M. Łazarska, Z. Ranachowski, J. Musiał, T. Tański, and Q. Jiang: *Materials*, 2025, vol. 18, p. 2198.
20. K. Nalepka, J. Tabin, J. Kawałko, A. Brodecki, P. Bała, and Z. Kowalewski: *Int. J. Plast.*, 2024, vol. 183, p. 104159.
21. H. Paul, J.H. Driver, A. Tarasek, W. Wajda, and M.M. Miszczyk: *Mater. Sci. Eng., A*, 2015, vol. 642, pp. 167–80.
22. K. Nalepka, B. Skoczeń, R. Schmidt, W. Zwolińska-Faryj, E. Schmidt, and R. Chulist: *Int. J. Plast*, 2024, vol. 177, p. 103994.